Foil Acceleration and Energy Transport

F. Amiranoff[1)], K. Eidmann, R. Fedosejevs[2)],
T. Kishimoto, A.G.M. Maaswinkel, R. Sigel,
Yung-lu Teng[3)], and S. Witkowski

MPQ 59 April 1982

MPQ-Report
59

MPQ

MAX-PLANCK-INSTITUT FÜR QUANTENOPTIK

8046 GARCHING BEI MÜNCHEN

MPQ 59 / 1982

Foil Acceleration and Energy Transport

F. Amiranoff[1], K. Eidmann, R. Fedosejevs[2],
T. Kishimoto, A.G.M. Maaswinkel, R. Sigel,
Yung-lu Teng[3], and S. Witkowski

Abstract

The last period of experiments at MPQ concentrated on the study of hydrodynamics and energy transport in laser produced plasmas. Thin low Z foil targets (10^{-5} - 10^{-3} g/cm^2) have been irradiated with 300 ps pulses from the iodine laser Asterix III (λ = 1.3 µm). Different diagnostics such as high speed photography, plasma-calorimetry, Ulbrichtsphere for laser light absorption measurements, and X-ray and ion techniques have been used. Results on the velocity and energy of the accelerated foil, pressure, ablation rate and the lateral spreading of energy were obtained for a wide intensity range 10^{12} - 10^{16} W/cm^2. The experimental data are compared with 1-D hydrodynamic calculations using different values of electron heat flux limitation.

Introduction: If a thin foil target is irradiated from one side by intense laser light a hot and dense plasma will form on the irradiated surface. Due to the high pressure exerted by the plasma onto the target material, a thin foil target may be accelerated to a high velocity. This acceleration process is of particular interest for laser fusion as well as for the more general possibility of accelerating macroscopic bodies to very high velocities.

In this paper we summarize a series of acceleration experiments with thin, low Z foil targets, performed during the last years in our laboratory using the iodine laser ASTERIX III. In these experiments we have measured the asymptotic velocity and the energy transfer to the accelerated foil material as a function of foil thickness over a wide range of inten-

Permanent address: 1) Ecole Polytechnique, Palaiseau (France), 2) University of Alberta, Edmonton (Canada), 3) Institute of Optics and Fine Mechanics, Shanghai (People's Republic of China)

sities from 10^{12} to nearly 10^{16} Wcm^{-2} incident intensity. If compared to theoretical models such data should yield information about the transport of energy from the absorption (critical density) region to the dense part of the target. We should mention that extensive studies of thin foil acceleration are also performed at NRL and other laboratories /1/.

Experimental set-up: The experiments were performed with the iodine laser Asterix III: wavelength 1.3 µm, pulse energy on target 100 - 150 J, pulse duration 300 ps (FWHM), focused with an aspherical f/2 lens to a minimum spot size of 60 µm diam. (half energy). The intensity on target was varied by placing the target at different distance from the beam waist or by attenuating the pulse energy. As targets thin plastic films ($C_6H_7O_{11}N_3$ (ρ = 1.6 g/cm^3) for d_F < 1 µm or $C_{16}O_3H_{14}$ (ρ = 1.18 g/cm^3) for d_F > 1 µm) in the thickness range d_F = 0.1 - 20 µm were used.

The simplified experimental scheme in Fig. 1 shows the calorimeter for measurement of energy transfer to the accelerated foil material, the high-speed photography diagnostics using a synchronized 10 ps dye-laser pulse for shadowgraphy and a 8-pinhole camera for x-ray imaging of the target. Other diagnostics (not shown) include an integrating sphere for absorption measurements, detectors for measurements of transmission of laser light through the target, a flat crystal Bragg spectrometer, an 8-channel absorbing foil spectrometer for continuous x-ray radiation, ion collectors and a Thomson parabola mass spectrometer.

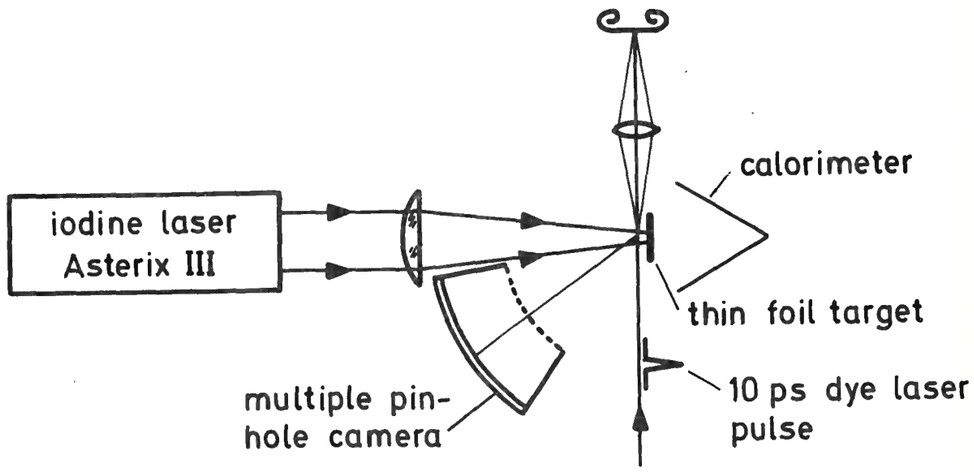

Fig. 1: Simplified experimental scheme

Experimental results: Fig. 2 shows the measured total reflectivity in the intensity range 10^{12} - 6 x 10^{15} Wcm^{-2}. The measurements were made with a 2 µm thick foil which is thicker than the ablated layer thickness

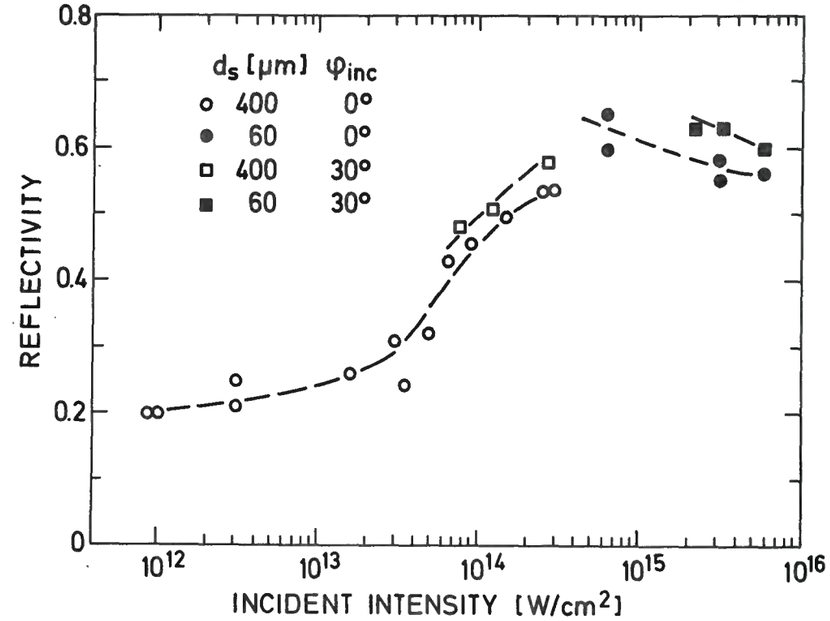

Fig. 2: Target reflectivity, integrated with an Ulbricht sphere over 2 π. d_s laser spot diameter, φ_{inc} angle of incidence.

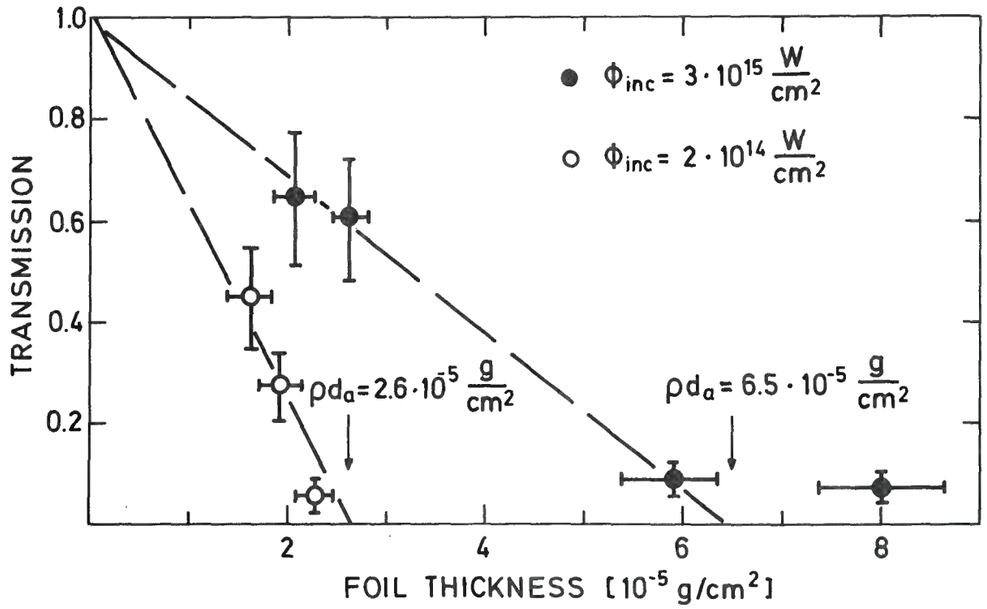

Fig. 3: Transmission of laser light through thin foil targets

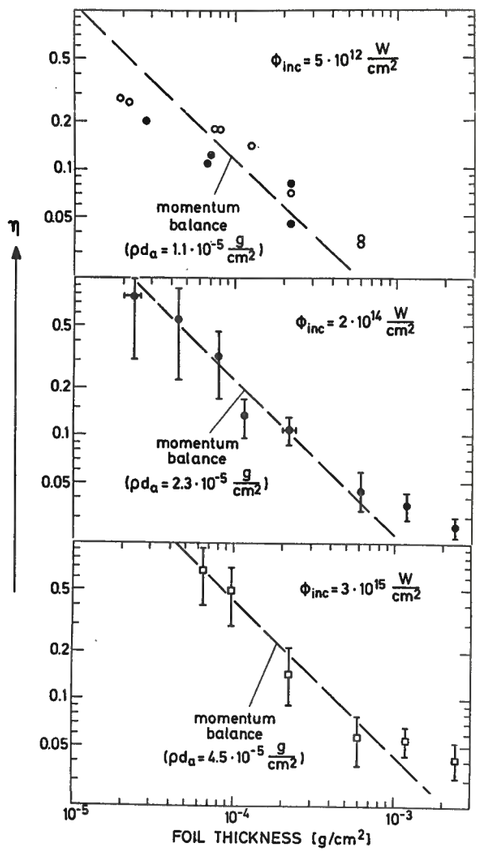

Fig. 4: Energy transfer to the accelerated foil material measured by calorimetry. η = calorimeter energy / absorbed laser energy.

d_a and does not burn through during the laser pulse. Transmission measurements of very thin films are shown in Fig. 3. They allow a determination of the ablated layer thickness d_a for the two different intensities as indicated in Fig. 3. A more detailed investigation of laser light reflection in this experiment has been published in /2a/.

The results of calorimeter measurements for three different intensities are shown in Fig. 4. The hydrodynamic efficiency η is defined by η = calorimeter energy / absorbed laser energy. For very thin foils (near burn through) η is high ($\eta \cong 0.5$); for thicker foils it decreases inversly proportional to the foil thickness. In the limit of very thick foils η saturates at $\eta \cong 0.03$ (η is then determined by the energy transfer to the shock wave in a thick target).

Shadowgrams obtained with the 10 ps dyelaser background illumination /2b/ are shown in Fig. 5. Shortly after the end of the laser pulse (Fig. 5b) the plasma cloud in front of the target is still visible; after several nanose-

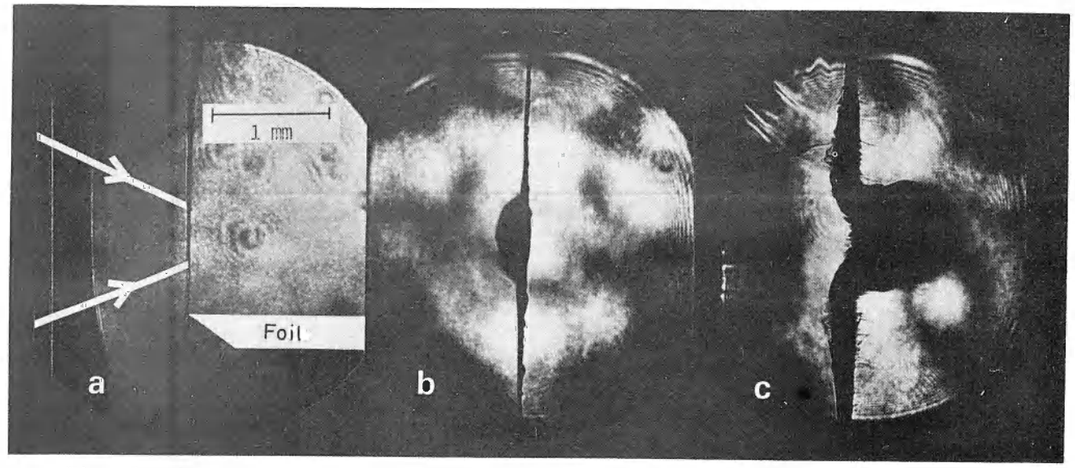

Fig. 5: Shadowgrams of thin foil targets obtained with 10 ps dyelaser background illumination. a) before irradiation b) 0.54 ns after maximum of iodine laser pulse c) after 6.4 ns. $\Phi_{inc} = 2 \times 10^{14}$ Wcm^{-2} (400 µm spot diam.). The foil strip is ~ 500 µm wide.

conds it has disappeared and the accelerated foil material has moved to the right.

With the dyelaser operated in the long pulse (~ 1 µs) mode it was also possible to follow the target motion in a single shot by streak photography (Fig. 6). The formation and decay of the plasma cloud on the irradiated front side as well as the acceleration phase followed by constant velocity motion on the rear side can clearly be seen. The asymptotic velocities of the foil determined by streak photography are shown in Fig. 7.

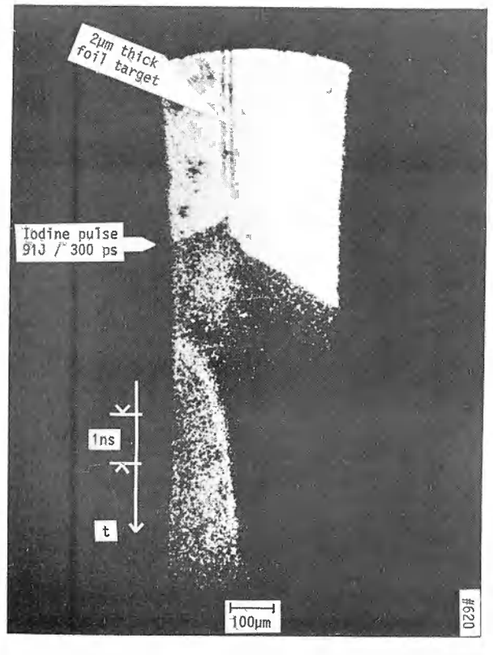

Fig. 6: Streak shadowgram of a 2 µm thick foil target obtained with long pulse background illumination.

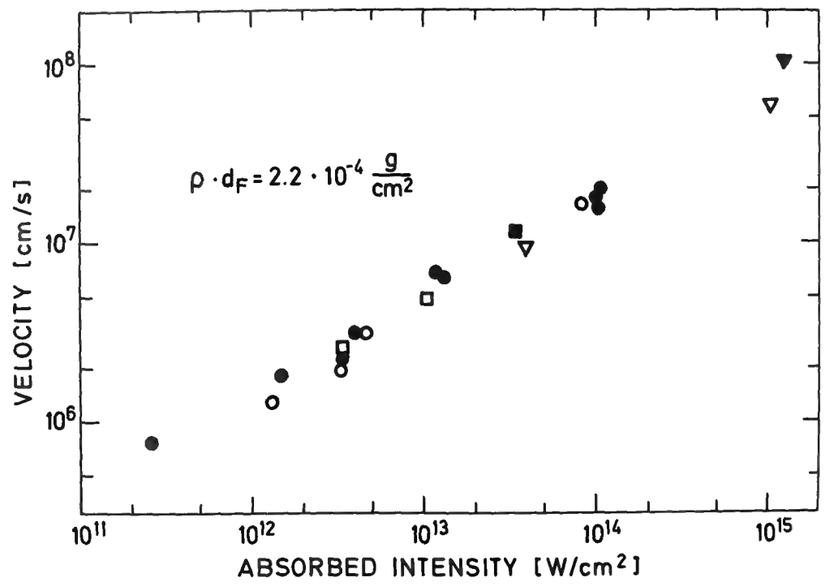

Fig. 7: Velocity of accelerated foil material as a function of absorbed intensity. ▼, ●, ■ : streak photography with laser spot diameter of 60, 400, and 1000 µm, respectively. ▽, ○, □ : calculated from calorimetry for the same spot diameters.

At the higest irradiations (irradiated area 60 µm diam., incident intensity $\Phi_{inc} \cong 3 \times 10^{15}$ Wcm^{-2}) several features of laser-plasma interaction become very pronounced which are less prominent or absent for medium and low intensity ($\Phi_{inc} \leqq 2 \times 10^{14}$ Wcm^{-2}). Shadowgraphs (Fig. 8) show that the irradiated foil strip explodes over a length of several millimeters i.e. a distance very much larger than the diameter of the irradiated area. This shows that a fraction of the absorbed energy is deposited outside the irradiated area.

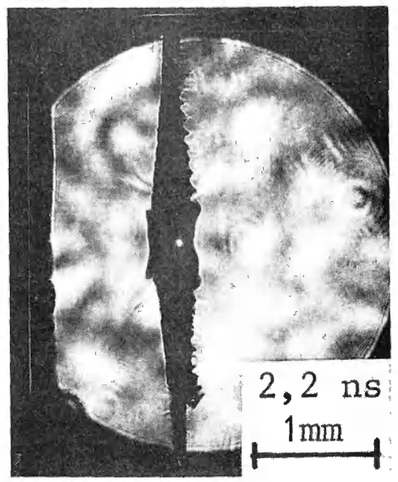

Fig. 8: Foil strip irradiated at high intensity (3×10^{15} Wcm^{-2}, 60 µm diam. spot). At 2.2 ns the target is seen to explode over the whole field of view.

As was reported earlier /2c/ massive plexiglas targets show internal breakdown (Fig. 9) indicating the existence of electrical fields in excess of 10^6 V/cm near the plasma cloud. The hard x-ray emission (5 - 50 keV) increases by nearly 3 orders of magnitude from 2×10^{14} to 5×10^{15} Wcm^{-2} suggesting that a significant fraction of the

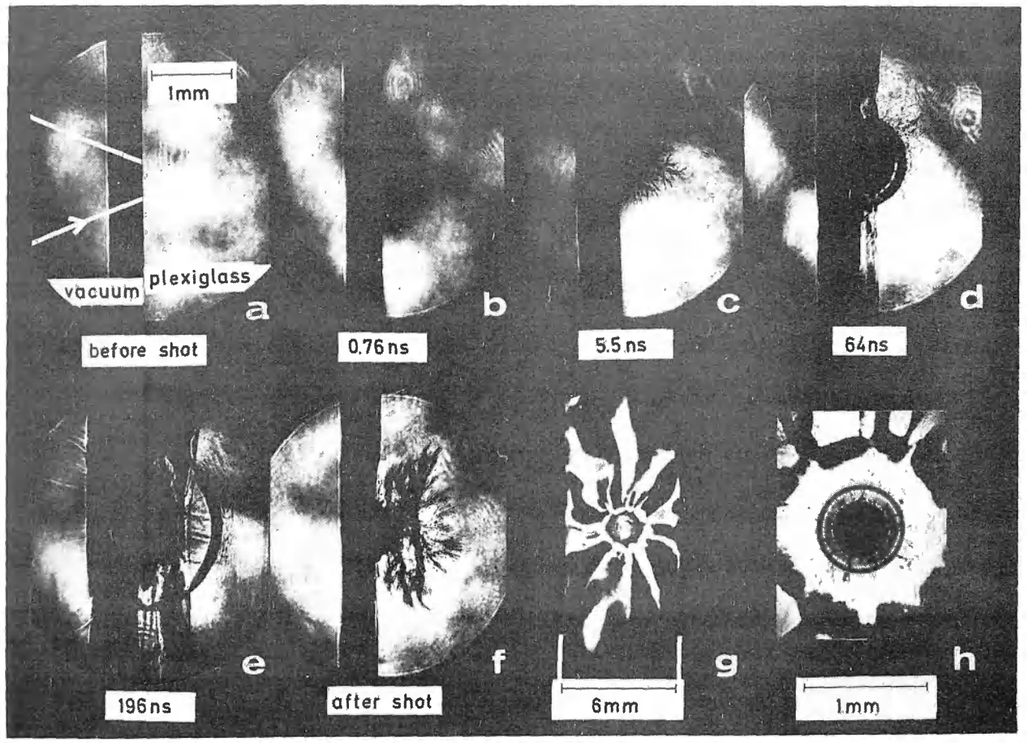

Fig. 9: Sequence of high-speed photographs showing the internal breakdown of a plexiglas target at a laser irradiance of 3×10^{15} Wcm^{-2}. a. Illustration of the interaction geometry. The vacuum/plexiglass interface is the right edge of the vertical dark band. The picture was taken prior to a laser shot. b. Formation of a dark cloud. c. Treelike discharge pattern. d, e. Appearance of a hemishperical shockwave. f. Permanent damage left in the target. g. Starlike surface damage on the front side of the target. h. Magnified detail of g showing laser-produced crater. From ref. /2c/.

absorbed energy is now coupled into fast electrons with a temperature $T_H \cong 20$ keV. In addition about 30 % of the absorbed energy are found in fast ions with velocities over 2×10^8 cm s^{-1} /2d/.

For the interpretation of the experiments it is particularly important to know what fraction of the absorbed energy is deposited remote from the irradiated area. Such a lateral energy transport might be caused by the fast electrons which can move without collisions in the

the rapidly expanding plasma cloud. A quantitative determination of remote fast electron energy deposition was made from spatially resolved pinhole photographs suitably filtered to isolate the contribution due to characteristic K_α radiation from the target material /3/. Fig. 10 shows examples obtained with a Vanadium target. The spread out emission is due to K_α emission excited by fast electrons with energies sufficient to remove an electron from the K - shell (5.5 keV for V). This is demonstrated by the difference between Fig. 10a and b which were obtained in the same shot. Filters in front of the pinholes were a 12.5 µm Ti foil and a 25 µm Sc foil, with a transmission of 0.62 and 6×10^{-3}, respectively, for V K_α radiation. Remote K_α emission is suppressed in Fig. 10b. In Fig. 10a and c it is seen that the fast electrons deposit their electrons preferentially at the edges of the target suggesting that the electron trajectories might be influenced by electric fields. On extended targets emission occurs in a ring zone (Fig. 10d). Possibly the area surrounding the irradiated spot is shielded by the toroidal megagauß magnetic fields known to exist in laser-produced plasmas. Similar observations have been made in CO_2 laser interaction experiments /4/.

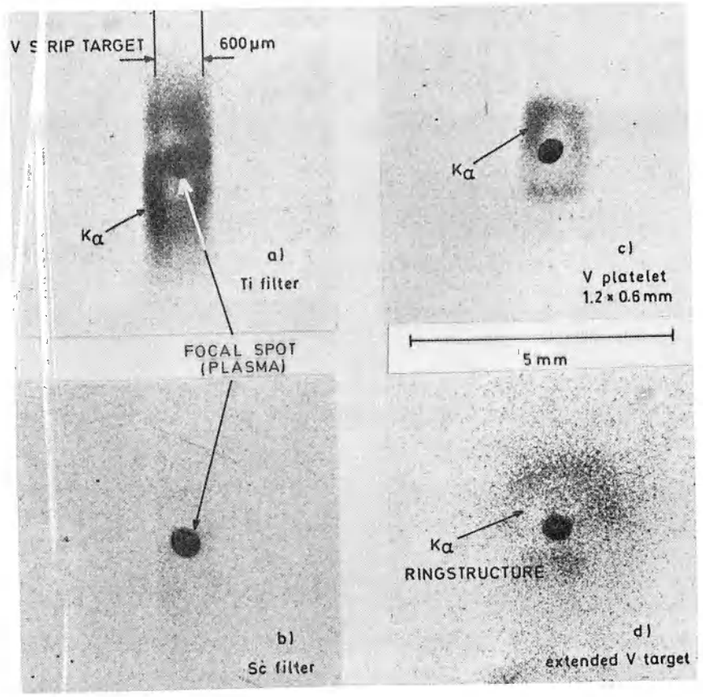

Fig. 10: x-ray pinhole photographs showing characteristic K_α radiation of the target excited by fast electrons spreading out from the focal spot.

From the observed K_α emission it was estimated that about 15 % of the absorbed energy are deposited remote from the irradiated area.

Interpretation of the experimental results: As a result of laser irradiation a layer with thickness d_a is ablated from the foil target with thickness d_F. In the most simple description we may assume that after the end of the acceleration phase the ablated mass and the rest mass of the foil move into apposite directions with purely kinetic energy. Then we obtain from momentum balance for the fractional energy transfer to the accelerated foil

$$\eta = \frac{d_a}{d_F} \qquad (1)$$

Using this relation the ablated mass has been determined from the calorimetric measurements of Fig. 4. The result is shown in Fig. 11 together with values obtained from transmission measurements (Fig. 3) and x-ray line spectroscopy on layered targets. The values obtained by these very different measurement methods agree within a factor two (a discussion of the remaining differences is outside the scope of this short paper).

The foil target is accelerated by the pressure p which is exerted by the laser heated plasma. The equation of motion for the foil with the instantaneous mass per unit aerea m/F is given by

$$p = \frac{m}{F}\,\frac{dv}{dt} \simeq \frac{\varrho d_F v}{\tau_{eff}} \qquad (2)$$

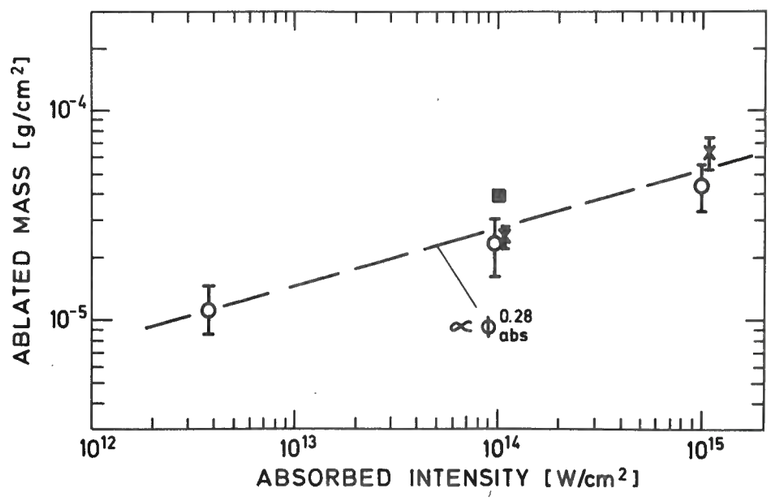

Fig. 11: Ablated mass determined from ○ calorimetry, x transmission of laser light, and ■ x-ray line spectroscopy with layered targets.

Using eq. (2) the pressure was determined from the high speed photographic data; either, using eq. (2) in its exact form, by differentiation (streak photographs) or, using the approximate form, from the asymptotic velocity (framing photographs) and an effective acceleration time $\tau_{eff} \cong$ 600 ps determined from the streak photographs. The mass loss of the foil

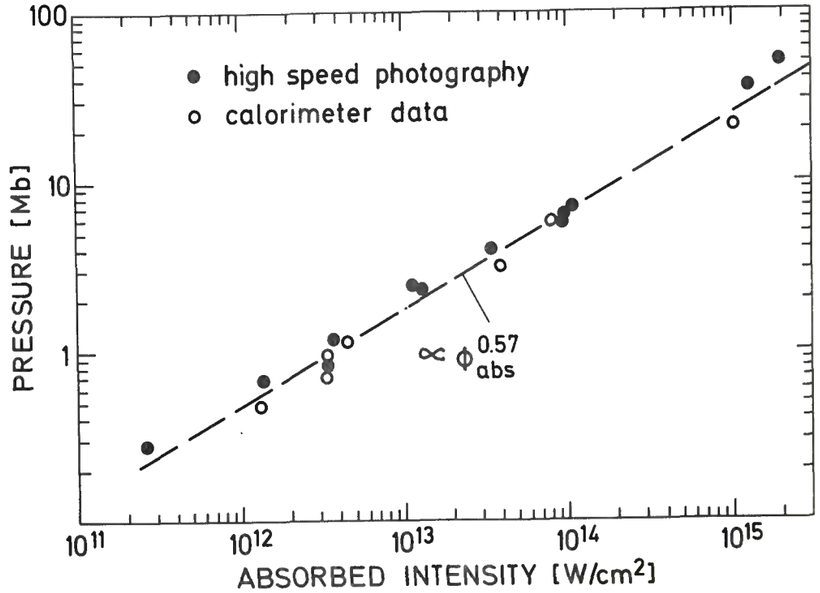

Fig. 12: Accelerating pressure as a function of absorbed intensity.

during irradiation was taken into account when necessary (thin foils with $d_F \leqq 2$ µm). The variation of pressure with intensity is shown in Fig. 12. It increases from 300 Kbar at 2.5 x 10^{11} W/cm^{-2} to 50 Mbar at 2 x 10^{15} Wcm^{-2} absorbed intensity.

It is interesting to note that the velocity of the accelerated material as measured directly by high-speed photography is consistent with the velocity determined from the calorimeter measurements if the assumption is made that the accelerated mass is determined by the laser spot diameter (note the corresponding data points in Fig. 7). This assumption is confirmed by the shadograms; also lateral spreading of energy was found to be , even at the highest intensities, only marginally important (15 % of absorbed energy). The consistency of these data also suggests that the rear velocity observed by streak photography is very close to the center of mass velocity of the foil. According to computer simulations this is expected for the 2 µm thick foil targets referred to in Fig. 7.

The macroscopic hydrodynamic quantities measured in the experiments depend on the microscopic processes occurring during laser-plasma interaction. Of particular importance here is the electron heat conductivity which controls the ablation process at the target surface. Numerical simulations of the foil acceleration process in comparison with the experi-

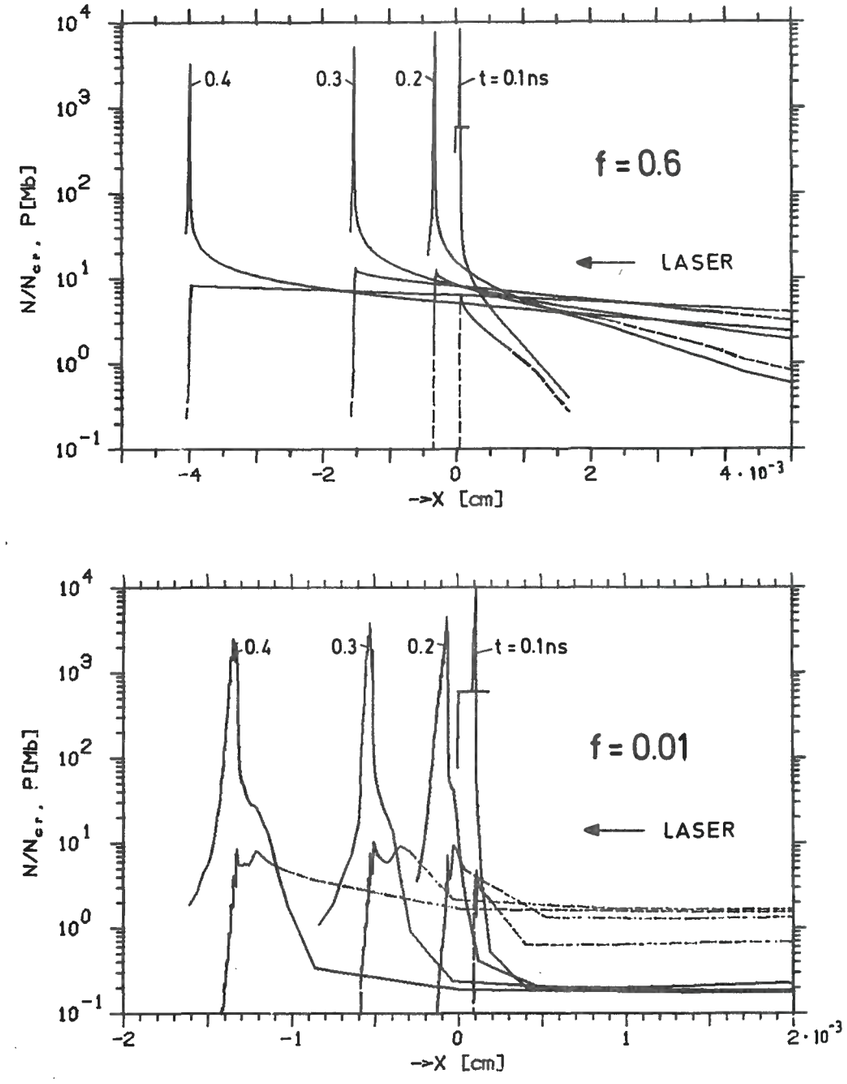

Fig. 13: 1D (planar) numerical simulation of foil acceleration with flux limit factor f = 0.6 and f = 0.01. Shown are the spatial variation of density (solid lines) and pressure (dashed lines) at various times during the laser pulse. Foil thickness 2.2 x 10^{-4} gcm^{-2}. ϕ_{abs} = 1 x 10^{14} Wcm^{-2}. Note the different spatial scale for the two cases.

mental results should allow to evaluate the validity of various assumptions on the heat conduction process.

We have simulated the experiments with a 1D hydrocode in planar geometry. The heat flux was modelled by

$$q = \mathrm{Min}\left\{q_{spitzer};\ f\, n_e \sqrt{kT_e / m_e}\ kT_e\right\} \qquad (3)$$

where the so-called flux limit factor f restricts the heat flux (f = 0.6 corresponds to the free-streaming limit). As an example Fig. 13 shows the simulation of a 2 µm foil irradiation experiment. Flux limitation with f = 0.01 results in a reduction of the final velocity by more than a factor two (note the enlarged scale in Fig. 13b). In Fig. 14 the calorimetric measurements are compared to simulations. With increasing intensity the experimental data fall on curves with stronger flux limitation (smaller f). Below ~ 10^{13} Wcm^{-2} no flux limitation is required. Though not further discussed here we should also mention that the simulations tolerate less than 5 % fast electron preheat.

Detailed simulations have shown that the concept of flux limitation (which uses only a single free parameter) is remarkably successful in

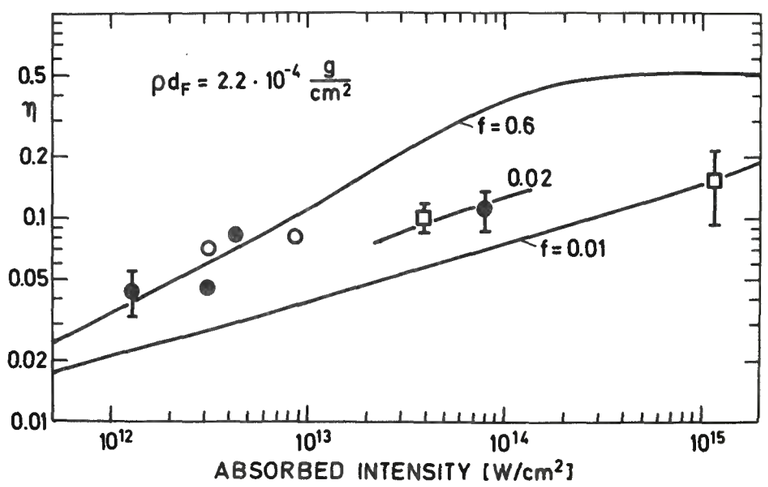

Fig. 14: Calculated and measured energy transfer to the accelerated foil material. □ 60 µm, ● 400 µm, ○ 1600 µm laser spot diameter.

fitting the experimental results. In using this concept in planar simulations one seeks to trace down the experimental observations to the microscopic heat conduction process. Apparently heat conduction in the plasma depends on the applied intensity.

Could the agreement thus obtained be fortuitous? Has the apparent reduction in heat conductivity perhaps to do with the fact that with increasing intensity the laser spot size has to be decreased and physical effects not existing in truly planar geometry become important?

We have no final answer to this question at the present time. Experiments at constant intensity, but different laser spot diameter (compare Fig. 7 and 14) show no dependence on spot diameter. Also, at the standard intensity of 2 x 10^{14} Wcm^{-2} (400 µm diam. spot), the interaction should be planar during the relatively short (300 ps) pulse; nevertheless strong flux limitation (f = 0.02) is required. On the other hand the complicated fast electron trajectories suggested by the K_α observations of Fig. 10, accompanied by fast ion losses and possibly the formation of magnetic fields, are high intensity phenomena which seem intimately connected with the small size of the laser spot. Their connection with the microscopic transport phenomena of the plasma is not known.

It seems that further progress towards a detailed understanding of the laser-target interaction physics needs more detailed investigations and also more powerful lasers for high intensity experiments close to the idealized geometry of theoretical calculations.

/1/ B.H. Ripin et al., Phys. Fluids 23, 1012 (1980); J. Grun, R. Decoste, B.H. Ripin, and J. Gardner, Appl. Phys. Lett. 39, 545 (1981); A. Raven, H. Azechi, T. Yamanaka, and C. Yamanaka, Phys. Rev. Lett. 47. 1049 (1981); Groupement de Recherches Coordonées Interaction Laser Matière, Ecole Polytechnique 91128 Palaiseau (France), Rapport d'Activité 1979; G. Thiell et al., CEA Limeil, 94190 Villeneuve-Saint Georges (France), presented at 14th Eclim (1980).

/2/ K. Eidmann, G. Brederlow, R. Brodmann, R. Petsch, R. Sigel, G. Tsakiris, R. Volk, and S. Witkowski, J. Phys. D: Appl. Phys., 12, L 145 (1979); Yung-lu Teng, R. Fedosejevs, R. Sigel, K. Eidmann, R. Petsch, and G. Spindler, Laboratory Report PLF 41 (1980), Projektgruppe für Laserforschung, D-8046 Garching (FRG); R. Fedosejevs, Yung-lu Teng, R. Sigel, K. Eidmann, and R. Petsch, J. Appl. Phys. 52, 4186 (1981); G.D. Tsakiris, K. Eidmann, R. Petsch, and R. Sigel, Phys. Rev. Lett. 46, 1202 (1981);

/3/ J.D. Hares, J.D. Kilkenny, M.H. Key, J.G. Lunney, Phys. Rev. Lett. 42, 1216 (1979);

/4/ P.A. Jaanimagi, N.A. Ebrahim, N.H. Burnett, C. Joshi, Appl. Phys. Lett. 38, 734 (1981).